

1 **PLASIM-GENIE v1.0: a new intermediate complexity**

2 **AOGCM**

3 P.B. Holden<sup>1</sup>, N.R. Edwards<sup>1</sup>, K. Fraedrich<sup>2</sup>, E. Kirk<sup>3</sup>, F. Lunkeit<sup>3</sup> and X. Zhu<sup>4</sup>

4 <sup>1</sup>Environment, Earth and Ecosystems, The Open University, Walton Hall, Milton  
5 Keynes, MK7 6AA, UK

6 <sup>2</sup>Max Planck Institute of Meteorology, KlimaCampus, Bundesstraße 53, 20146  
7 Hamburg, Germany

8 <sup>3</sup>Meteorological Institute, University of Hamburg, Bundesstraße 55, 20146  
9 Hamburg, Germany

10 <sup>4</sup>Center for Earth System Research and Sustainability (CEN), University of  
11 Hamburg, Grindelberg 5, 20144 Hamburg, Germany

12

13 **Abstract**

14 We describe the development, tuning and climate of PLASIM-GENIE, a new  
15 intermediate complexity Atmosphere-Ocean Global Climate Model (AOGCM),  
16 built by coupling the Planet Simulator to the ocean, sea-ice and land-surface  
17 components of the GENIE Earth system model. PLASIM-GENIE supersedes  
18 “GENIE-2”, a coupling of GENIE to the Reading IGCM. The primitive-equation  
19 atmosphere includes chaotic, 3D motion and interactive radiation and clouds,  
20 and dominates the computational load compared to the relatively simpler  
21 frictional-geostrophic ocean, which neglects momentum advection. The model is  
22 most appropriate for long-timescale or large ensemble studies where numerical  
23 efficiency is prioritised, but lack of data necessitates an internally consistent,  
24 coupled calculation of both oceanic and atmospheric fields. A 1,000-year  
25 simulation with PLASIM-GENIE requires approximately two weeks on a single node  
26 of a 2.1GHz AMD 6172 CPU. We demonstrate the tractability of PLASIM-GENIE  
27 ensembles by deriving a “subjective” tuning of the model with a 50-member  
28 ensemble of 1,000-year simulations. The simulated climate is presented considering  
29 (i) global fields of seasonal surface air temperature, precipitation, wind, solar and  
30 thermal radiation, with comparisons to reanalysis data; (ii) vegetation carbon, soil  
31 moisture and aridity index; (iii) sea surface temperature, salinity and **ocean**  
32 **circulation**. Considering its resolution PLASIM-GENIE reproduces the main features

33 of the climate system well and demonstrates usefulness for a wide range of  
34 applications.

35

## 36 **1. Introduction**

37 The Grid-ENabled Integrated Earth system model (GENIE, Lenton et al 2007) has  
38 been developed as a modular framework that allows a spectrum of intermediate  
39 complexity Earth system models to be created by selecting different options for  
40 the various climate and carbon cycle components. Earth system models created  
41 within GENIE have been configured for published studies spanning a wide range  
42 of geological epochs across Paleozoic, Mesozoic and Cenozoic eras. GENIE  
43 framework models are normally capable of integration over multi-millennial  
44 timescales and several of the published studies have involved millions of years of  
45 simulation time combining long runs and large ensembles. The framework has  
46 been designed to be modular to facilitate the coupling of more complex  
47 component modules as available computing power increases.

48

49 Almost invariably, applications of GENIE have used configurations that represent  
50 the atmosphere with a computationally fast energy-moisture-balance-model  
51 (EMBM, Fanning and Weaver 1996). These configurations are generically named  
52 "GENIE-1". Although adequate for many purposes, especially in the context of  
53 global biogeochemical modelling, an EMBM introduces significant structural  
54 weaknesses to (or even rules out) a range of applications. Diffusive single-layer  
55 moisture transport leads to poor precipitation fields that cannot, for instance,  
56 represent convective precipitation or monsoon dynamics. The EMBM applies  
57 prescribed surface wind fields (Edwards and Marsh 2005), defined either from  
58 climatology or from outputs of more complex models, so that dynamic ocean  
59 feedbacks are restricted to the thermohaline circulation. Clouds are represented  
60 through a prescribed albedo field (Lenton et al 2006) and a spatially uniform  
61 adjustment to outgoing longwave radiation OLR (Holden et al 2010), while  
62 uncertain cloud feedbacks on the radiative balance in a changing climate are  
63 represented through a globally uniform temperature dependent adjustment to  
64 OLR (Matthews and Caldeira 2007, Holden et al 2010).

65

66 In an effort to address these shortcomings, the Reading Intermediate General  
67 Circulation Model (IGCM3.1, de Forster et al 2000), a 3D dynamical model of the  
68 atmosphere, was coupled into GENIE (Annan et al 2005, Lenton et al 2007).  
69 Unfortunately this realization of the model “GENIE-2” proved problematic and  
70 has only been applied once since these early studies (Holden and Edwards  
71 2010). The coupling with the slab-ocean model was found to exhibit poor  
72 precipitation fields, apparently due to structural deficiencies in the convection  
73 routine (Annan et al 2005). The coupling with the 3D frictional geostrophic  
74 ocean model GOLDSTEIN displays a patchwork-instability and exhibits a low bias  
75 in precipitation over ocean. GENIE-2 requires a large moisture flux correction  
76 (0.79Sv, reversing the sign of the simulated flux) to reconcile freshwater  
77 transport from the Atlantic to the Pacific with reanalysis data (Lenton et al 2007)  
78 and generate an Atlantic overturning circulation. A further shortcoming is that,  
79 on account of technical complications discussed in Section 3.3, the IGCM was not  
80 coupled to the dynamic sea-ice module GOLDSTEINSEAICE, but only to the slab  
81 sea-ice module<sup>1</sup>.

82

83 GENIE-1 has been applied to a wide range of studies, including participation in  
84 the [Earth System Models of Intermediate Complexity \(EMIC\)](#) inter-comparisons  
85 that were performed for the two most recent IPCC reports (Plattner et al 2008,  
86 Zickfeld et al 2013). Although GENIE studies have generally addressed ocean  
87 physics, ocean biogeochemistry and the global carbon cycle, a more recent focus  
88 has been the development of emulators for climate impact assessment (e.g.  
89 Labriet et al 2013, Mercure et al 2014). This application is poorly suited to highly  
90 simplified atmospheric models such as the EMBM. Although the emulation  
91 techniques were developed from GENIE-2 simulations (Holden and Edwards  
92 2010), this first-generation emulator was not considered sufficiently robust for  
93 applications given the poor climatology of the underlying simulator. Instead, a

---

<sup>1</sup> The GENIE slab sea-ice module assumes a fixed thickness (2m), heat capacity and albedo (0.6). A grid cell becomes completely ice covered when the surface temperature falls below -2°C, with surface temperature evolving according to the energy flux balance. Sea-ice dynamics are neglected and there is no interaction with the hydrological cycle.

<sup>2</sup> The PLASIM sea-ice model is based on the thermodynamic model of Semtner (1976). It neglects dynamics. Spatio-temporal energy flux corrections are

94 second-generation emulator (Holden et al 2014) was developed using the Planet  
95 Simulator PLASIM (Fraedrich 2012).

96  
97 PLASIM is a reduced complexity AGCM, with the 3D primitive equation **Portable**  
98 **University Model of the Atmosphere (PUMA)** at its core (Fraedrich et al 2005). We  
99 use the PLASIM-ENTS (**Efficient Numerical Terrestrial Scheme**) implementation  
100 (Holden et al 2014), which incorporates the same land surface model as GENIE.  
101 Complementary to GENIE-1, PLASIM has been applied in a range of atmospheric  
102 studies, for instance investigating the global entropy budget (Fraedrich and  
103 Lunkeit, 2008), double **Inter-Tropical Convergence Zone** dynamics in an  
104 aquaplanet (Dahms et al, 2011), the Permian climate (Roscher et al, 2011) and a  
105 snowball Earth (Micheels and Montenari, 2008). However, although PLASIM  
106 simulates vastly better climatology than the EMBM of GENIE-1, it lacks dynamic  
107 representations of ocean and sea ice (and does not model the carbon cycle) so it  
108 too neglects important Earth system feedbacks.

109  
110 We here describe the implementation of a coupling of PLASIM-ENTS to the  
111 physical components of the GENIE framework. The coupled model “PLASIM-  
112 GENIE” has been developed to join the limited number of models that bridge the  
113 gap between EMICs with simplified atmospheric dynamics and state of the art  
114 AOGCMs. We are aware of three AOGCMs of comparable complexity with  
115 primitive equation atmospheric dynamics: FAMOUS (**Fast Met Office/UK**  
116 **Universities Simulator**), the reduced resolution implementation of the **Hadley**  
117 **Centre Coupled Model** HadCM3, which simulates 1,000 years in approximately  
118 ten days on eight CPUs (Williams et al, 2013), SPEEDO (**Speedy-Ocean**),  
119 comprising a T30 spectral atmosphere with simplified parameterizations  
120 (Molteni 2003) coupled to a primitive equation ocean model, which simulates  
121 1,000 years in approximately two weeks on a 3GHz dual core Intel E6850 CPU  
122 (Severijns and Hazeleger, 2010) and OSUVic (**Oregon State University Victoria**), a  
123 coupling of PLASIM to the UVic Earth system model (Schmittner et al, 2010). A  
124 1,000-year simulation with PLASIM-GENIE requires approximately two weeks on a  
125 single node of a 2.1GHz AMD 6172 CPU.

126

127 State of the art climate models operate at the limit of available computing power,  
128 so that very few simulations can be performed with these models. An important  
129 motivation for intermediate complexity models is for the evaluation of  
130 uncertainty. We here demonstrate the tractability of PLASIM-GENIE ensembles by  
131 tuning the model with a 50-member ensemble of 1,000-year simulations.

132

## 133 **2. Component Modules**

134

### 135 **2.1 PLASIM-ENTS**

136 PLASIM (Fraedrich 2012) is a reduced complexity AGCM, with the 3D primitive  
137 equation atmosphere model PUMA at its core (Fraedrich et al 2005). PLASIM is  
138 described in detail in Lunkeit et al (2007) and references therein. We summarise  
139 briefly here. The atmospheric dynamics are solved using the spectral transform  
140 method, formulated for temperature, specific humidity, log surface pressure,  
141 divergence and vorticity. The short wave radiation scheme separates solar radiation  
142 into two bands,  $\lambda < 0.75\mu\text{m}$  (with cloud scattering, ozone absorption and Rayleigh  
143 scattering) and  $\lambda > 0.75\mu\text{m}$  (with cloud scattering, cloud absorption and water  
144 vapour absorption). The long wave radiation scheme uses the broad band emissivity  
145 method, with the (greenhouse gas) effect of water vapour, carbon dioxide and ozone  
146 included in the calculation of emissivity. Ozone concentration is prescribed with an  
147 analytic spatio-temporal distribution. Cloud emissivity is calculated from the cloud  
148 liquid water content. Fractional cloud cover is diagnosed from relative humidity  
149 (stratiform clouds) and from the convective precipitation rate (convective clouds).  
150 Other parameterised processes include large-scale precipitation, moist convection  
151 (both cumulus and shallow), dry convection, boundary layer heat fluxes, vertical  
152 diffusion (to represent unresolved turbulent exchange) and horizontal diffusion  
153 (applied to selectively dampen short wavelengths in spectral space).

154

155 The land surface scheme (previously the Simulator for Biospheric Aspects, SimBA,  
156 Kleidon et al 2005) was modified (Holden et al 2014) to use GENIE's efficient  
157 numerical terrestrial scheme ENTS (Williamson et al 2006), partly in anticipation of  
158 this coupling to GENIE. ENTS models vegetative and soil carbon densities, assuming  
159 a single plant functional type that has a doubled-peaked temperature response

160 (representing boreal and tropical forest). In addition to temperature, the rate of  
161 photosynthesis depends upon the atmospheric CO<sub>2</sub> concentration and on soil moisture  
162 availability. ENTS includes a parameterisation of self-shading, so that new  
163 photosynthetic production is channelled into leaf litter when fractional vegetation  
164 coverage approaches one and the canopy closes. Land surface albedo, moisture bucket  
165 capacity and surface roughness are parameterised in terms of the simulated carbon  
166 pool densities. We note that although the state variables simulated by ENTS are the  
167 vegetation and soil carbon densities, we have not coupled PLASIM-GENIE to the  
168 GENIE-1 carbon cycle; this extension is straightforward in principle and will be  
169 addressed in future work. In this coupling, ENTS can be run in a diagnostic mode  
170 (setting parameter *nbiome*=2), simulating dynamically changing terrestrial carbon  
171 pools without affecting the climate state.

172

173 PLASIM includes flux-corrected slab ocean and sea-ice models<sup>2</sup>. The coupling  
174 described here (Section 3) replaces these simple models with the 3D dynamical ocean  
175 model GOLDSTEIN and the thermodynamic-dynamical sea ice model  
176 GOLDSTEINSEAICE.

177

## 178 **2.2 GOLDSTEIN**

179 GOLDSTEIN is a 3D frictional-geostrophic ocean model (Edwards and Marsh,  
180 2005; Marsh et al, 2011). GOLDSTEIN is dynamically similar to classical GCMs,  
181 except that it neglects momentum advection and acceleration. Barotropic flow  
182 around Antarctica is derived from linear constraints that arise from integrating  
183 the depth-averaged momentum equations; we here neglect flow through other  
184 straits. Several modifications to the default GOLDSTEIN can be enabled; here we  
185 apply the modified equation of state that includes a density adjustment for  
186 thermobaricity given by  $2.5 \times 10^{-5} Tz \text{ kgm}^{-3}$ , where  $T$  is temperature (°C) and  $z$  is  
187 height i.e. negative depth (m), and the enhanced diapycnal mixing scheme  
188 (Oliver and Edwards, 2008).

189

## 190 **2.3 GOLDSTEIN SEA ICE**

191 GOLDSTEINSEAICE (Edwards and Marsh, 2005) solves for the fraction of the  
192 ocean surface covered by ice within a grid cell and for the average sea-ice height.  
193 A diagnostic equation is solved for the ice surface temperature. Growth or decay  
194 of sea ice depends on the net heat flux into the ice (Semtner, 1976; Hibler 1979);  
195 sea-ice dynamics consists of advection by surface currents and diffusion. The  
196 thermodynamics of GOLDSTEINSEAICE are summarized in detail in Section 3.3.  
197

### 198 **3. Coupling methodology**

199 A schematic of the PLASIM-ENTS/GOLDSTEIN/GOLDSTEINSEAICE ‘pl\_go\_gs’  
200 coupling is illustrated in Figure 1.  
201

202 In order to avoid the need for interpolation, the coupling was set up to require  
203 the three models have matched horizontal grids. PLASIM has previously been  
204 configured for T21, T31 and T42 resolutions. Here we restrict the coupling to  
205 T21 and use the matched 64x32 GOLDSTEIN grid (Lenton et al 2007). PLASIM  
206 vertical resolution is 10 levels. GOLDSTEIN depth resolution is 32 levels, with  
207 bathymetry defined at the resolution of the 8 level configuration. Extension to  
208 other resolutions (horizontal or vertical) is straightforward in principle.  
209

210 The computational demands of the coupled model, simulating 75 years per day on a  
211 single node of a 256Gb 2.1GHz AMD 6172 CPU, are dominated by PLASIM (98%).  
212 The computational demands of PLASIM are dominated by diabatic processes (~76%),  
213 in particular by radiation (~43%) and precipitation (~16%). We note that the modular  
214 structure of PLASIM means that replacing the radiation scheme with, for example, a  
215 computationally fast semi-grey scheme (Frierson et al 2006) would be relatively  
216 straightforward. An efficient convective adjustment scheme (Betts and Miller 1986) is  
217 already available as an alternative to the default moisture budget scheme (Kuo 1965,  
218 1974).  
219

#### 220 **3.1 PLASIM-ENTS**

---

<sup>2</sup> The PLASIM sea-ice model is based on the thermodynamic model of Semtner (1976). It neglects dynamics. Spatio-temporal energy flux corrections are diagnosed from comparison with observed present-day sea-ice thickness.

221 The choice was made to preserve the coupled PLASIM-ENTS model in its entirety.  
222 The slab ocean and sea ice modules are retained only to provide boundary conditions;  
223 their state variables are over-written with GOLDSTEIN and GOLDSTEINSEAICE  
224 outputs, effectively negating the very simple dynamics of these models. This  
225 simplifies the coupling because the energy and moisture flux calculations are already  
226 made within PLASIM. The changes needed to PLASIM with this approach are  
227 therefore kept to a minimum, consisting of prescribing the slab ocean with  
228 GOLDSTEIN distributions of sea surface temperature and the slab sea-ice with  
229 GOLDSTEINSEAICE distributions of sea-ice fractional coverage, height, surface  
230 temperature and albedo. Furthermore, although GENIE contains a stand-alone version  
231 of the land surface module ENTS, the decision was taken to leave the existing  
232 PLASIM-ENTS coupling in place. Future work may separate the PLASIM and ENTS  
233 modules. The primary motivation for this would be modularity. Notably GENIEfied  
234 ENTS is coupled to the global carbon cycle (Lenton et al 2006) and has been enabled  
235 to simulate the effects of anthropogenic land use change (Holden et al 2013a).

236

### 237 **3.2 GOLDSTEIN**

238 No changes were made to GOLDSTEIN. Surface wind stress, net energy and net  
239 moisture fluxes are supplied from PLASIM, modified by sea ice where relevant. We  
240 note that we use a PLASIM time step of 45 minutes and a GOLDSTEIN time step of  
241 12 hours, with coupling inputs averaged over the previous 16 PLASIM time steps (12  
242 hours).

243

### 244 **3.3 GOLDSTEINSEAICE**

245 In GENIE-1 the thermodynamics of GOLDSTEINSEAICE are calculated within the  
246 EMBM, and coupling to alternative model atmospheres is not possible with this  
247 model structure. To enable a PLASIM-GOLDSTEINSEAICE coupling we have  
248 developed a stand-alone sea-ice thermodynamics routine.

249

250 Time-averaged incoming energy fluxes and atmospheric boundary conditions  
251 are supplied to the new ice surface flux (ICE-SURFLUX) routine from PLASIM.  
252 Sea surface temperature and salinity, sea-ice height and fractional sea-ice  
253 coverage are provided from the previous GOLDSTEIN/SEAICE time step.



254

255 ICE-SURFLUX closely follows the formulation of Edwards and Marsh (2005),  
256 where it is described in some detail. We summarize the approach here. Sea ice is  
257 assumed to have no heat capacity, so that the heat flux exchanged with the  
258 atmosphere equals the heat flux through the ice, thereby defining the vertical  
259 temperature gradient across the ice. The temperature at the sea-ice base is  
260 assumed equal to the salinity-dependent freezing point of the surface ocean, so  
261 that the ice-surface temperature is the remaining unknown. Now we need to  
262 derive the net heat flux from the atmosphere. Incoming radiative fluxes are  
263 provided by PLASIM; outgoing radiative fluxes, and sensible and latent heat  
264 fluxes are dependent upon the surface temperature of the sea ice, together with  
265 atmospheric boundary conditions. These relationships together imply an ice-  
266 surface temperature (and the associated atmospheric heat flux) that balances the  
267 heat budget, which is solved for with a Newton-Raphson algorithm. The heat flux  
268 exchanged with the ocean is implied by the temperature differential between the  
269 sea-ice base (freezing point) and the surface ocean. The difference between the  
270 heat flux exchanged with the atmosphere and with the ocean is consumed by  
271 creating or melting ice.

272

273 The diagnosed energy and moisture fluxes are not passed to PLASIM. Instead, in  
274 order to achieve energy and moisture conservation, PLASIM transfer coefficients  
275 are used in the calculation of sensible heat and sublimation during the Newton-  
276 Raphson step. This ensures that net fluxes calculated in PLASIM (which use the  
277 sea-ice temperature and albedo derived in ICE-SURFLUX) will be consistent with  
278 those calculated in ICE-SURFLUX, but does not guarantee perfect conservation.  
279 Conservation errors arise through differential time-stepping (the averaging of  
280 non-linear flux terms over 16 PLASIM time steps) and also because PLASIM does  
281 not explicitly account for sea-ice leads; ICE-SURFLUX separately accounts for  
282 ocean and sea-ice in a partially covered gridcell, but PLASIM fluxes are derived  
283 from weighted average surface properties<sup>3</sup>. To evaluate the magnitude of the

---

<sup>3</sup> A drift over the 2,000-year spin-up simulation is apparent in the 6<sup>th</sup> significant figure of global averaged salinity, likely also a consequence of the neglect of sea-ice leads in PLASIM and the differential time-stepping. While this modest failure

284 conservation errors, we consider all of the sea-ice covered grid cells at each time  
285 step across a year of the spun-up model. The energy conservation error across  
286 these 152,495 data points is  $0.1 \pm 1.0 \text{ Wm}^{-2}$  ( $1\sigma$ ). We note that the PLASIM  
287 atmosphere does not precisely conserve energy, as illustrated by Hoskins and  
288 Simmons (1975) for a similar dry dynamical core. The largest effect in PLASIM  
289 comes from the conversion from potential to kinetic energy. This conversion  
290 cannot be formulated in a conservative manner in the semi-spectral scheme  
291 since it involves triple products while the (Gaussian) grid only allows for the  
292 conservation of quadratic quantities. The top-of-atmosphere energy balance  
293 converges to  $-0.7 \text{ Wm}^{-2}$  in both the coupled and stand-alone versions of PLASIM,  
294 dominating over the conservation errors of ICE-SURFLUX.

295

296 Sea-ice growth rates are provided to GOLDSTEINSEAICE, which derives updated  
297 sea-ice distributions, considering both thermodynamics and dynamics  
298 (advection and diffusion). The updated sea-ice distribution is provided to  
299 PLASIM and the associated freshwater exchange with the ocean is provided to  
300 GOLDSTEIN.

301

## 302 **4. Tuning methodology**

303 Our approach for the selection of a tuned set of parameter values was to retain  
304 the existing tunings of models where possible (for exceptions see Section 4.1)  
305 and to only consider the parametric uncertainty of GOLDSTEIN. The motivation  
306 was that both PLASIM (Lunkeit et al 2007) and ENTS (Williamson et al 2006)  
307 have already been tuned to reproduce observations when forced with  
308 climatology<sup>4</sup>. In contrast, existing GOLDSTEIN tunings have been developed  
309 within a coupled atmosphere-ocean model, usually the EMBM atmosphere. We  
310 anticipated that a tuning of GOLDSTEIN that reproduces the main features of  
311 global ocean circulation when coupled to climatologically tuned PLASIM-ENTS  
312 would likely provide a good representation of observed climatology in general.

---

of moisture conservation is negligible for the physical model, it will be revisited for the carbon cycle coupling in order to ensure conservation of biogeochemical tracers.

313

314 We performed a 50-member ensemble of 1,000-year preindustrial spin-up  
315 simulations varying six GOLDSTEIN parameters, in the expectation that some  
316 subset of ensemble members would produce reasonable climate states from  
317 which we could select a tuned model. (Failure in this regard would have  
318 necessitated the application of more sophisticated statistical techniques for  
319 searching parameter input space).

320

#### 321 **4.1 Ensemble design**

322 Parameters from modules other than GOLDSTEIN were all fixed. However, some  
323 were changed from their default values (or are recently introduced  
324 parameterisations that are not associated with tuned defaults). These choices  
325 were made on the basis of exploratory simulations:

326 i) The uncertain effect of clouds on long wave radiation is controlled  
327 through the dependence of cloud emissivity  $A$  on the mass absorption  
328 factor  $k$  “acllwr”, following Slingo and Slingo (1991):

$$A = 1 - e^{-\beta kW}$$

329 where  $\beta = 1.66$  is the diffusivity factor and  $W$  the cloud liquid water  
330 path. The mass absorption factor was found to exert the strongest  
331 control on surface air temperature of the 22 key model parameters  
332 considered in PLASIM-ENTS ensembles (Holden et al 2014). The value  
333 was increased from default  $k = 0.1$  to  $0.2m^2g^{-1}$ , estimated to yield a  
334 simulated global average surface air temperature of approximately  
335  $14^\circ\text{C}$  in conjunction with parameter choices (ii) to (v) below.

336 ii) The PLASIM parameter *albseamax* defines the latitudinal variation of  
337 ocean albedo (Holden et al 2014),

$$\alpha_s = \alpha_{s0} + 0.5\alpha_{s1}[1 - \cos(2\varphi)]$$

338 where the ocean albedo  $\alpha_s$  is expressed in terms of latitude  $\varphi$ , the albedo  
339 at the equator  $\alpha_{s0} = 0.069$  and the parameter that controls latitudinal  
340 variability  $\alpha_{s1}$ . The calculated albedo is applied to both direct and  
341 scattered radiation. A high value ( $\alpha_{s1} = 0.4$ ) was favoured for

---

<sup>4</sup> The diurnal cycle is switched off in these simulations, reflecting the default

342 *albseamax*, leading to cooler high latitude ocean and favouring  
343 increased Southern Ocean sea-ice and deep-water formation, which  
344 both tended to be too low with default parameters.

345 iii) Sea ice is transported through advection and Laplacian diffusion  
346 (Edwards and Marsh, 2005), the latter taking the place of a detailed  
347 representation of unresolved advection and rheological processes.  
348 Sea-ice diffusivity (*SID*) influences **Antarctic Bottom Water (AABW)**  
349 formation by controlling the rate at which new ice is created, and  
350 hence the strength of brine rejection (Holden et al 2013b). A high  
351 value was favoured, again to strengthen deep-water formation, but  
352 values greater than  $15,000 \text{ m}^2\text{s}^{-1}$  were found to lead to numerical  
353 instabilities in this model and *SID* was fixed at this value.

354 iv) The standard PLASIM expression for the dependence of sea ice albedo  
355  $\alpha_i$  on surface air temperature is used

$$\alpha_i = 0.5 - 0.025T_{air}$$

356 where  $T_{air}$  is the surface air temperature ( $^{\circ}\text{C}$ ). PLASIM restricts the  
357 maximum albedo to 0.7 ( $T_{air} \leq -8^{\circ}\text{C}$ ). In PLASIM-GENIE we  
358 additionally restrict the minimum albedo, to 0.5 ( $T_{air} \geq 0^{\circ}\text{C}$ ).

359 v) The PLASIM-ENTS dependency of photosynthesis on soil moisture is

$$f_2(W_s) = \{(W_s/W_s^*) - q_{th}\}/\{0.75 - q_{th}\}$$

360 The parameter  $q_{th}$  (*qthresh*) was set to 0.1, allowing the development  
361 of vegetation in semi-arid regions (Holden et al 2014).

362

363 The ensemble was generated using a 50x6 maximin latin hypercube design,  
364 varying six GOLDSTEIN parameters, listed in Table 1 and varied over ranges  
365 considered to reflect the plausible range for each parameter (Holden et al 2013b  
366 and references therein). The six varied parameters are isopycnal and diapycnal  
367 diffusivities, a parameter *OP1* that controls the depth profile of diapycnal  
368 diffusivity (see below), the frictional drag coefficient (GOLDSTEIN is based upon  
369 the thermocline equations with the addition of a linear drag term in the  
370 horizontal momentum equations, Edwards et al 1998), wind stress scaling (a

---

assumption for both the PLASIM and ENTS tunings.

371 linear scaling of the surface wind-stress is applied to compensate for the energy  
372 dissipated by frictional drag), and an Atlantic-Pacific moisture flux adjustment.

373

374 Diapycnal diffusivity is stratification-dependent (Oliver and Edwards, 2008),  
375 given by

$$k_v = k_{v0} p_0(z)^\gamma \left( \frac{\Delta\rho_0(z)}{\Delta\rho(z)} \right)$$

376 where  $k_{v0}$  (reference diapycnal diffusivity) and  $\gamma$  (*OP1*) are varied across the  
377 ensemble (Table 1),  $p_0(z)$  is a reference profile (exponentially growing with  
378 depth and equal to 1 at 2500m),  $\Delta\rho_0(z)$  a reference vertical density gradient  
379 profile and  $\Delta\rho(z)$  the local simulated vertical density gradient.

380

381 Two ensemble parameters merit particular discussion here:

382

#### 383 **4.1.1 APM**

384 *APM* is a flux adjustment that transports moisture from the Atlantic to the Pacific,  
385 originally developed for the EMBM coupling (Edwards and Marsh, 2005). The  
386 default flux adjustment (0.32Sv) is subdivided into three latitude bands  
387 reflecting the observed Atlantic-Pacific moisture transport (Oort, 1983): -0.03Sv  
388 south of 20°S, 0.17Sv in the tropical zone 20°S to 24°N, and 0.18Sv north of 24°N.  
389 Exploratory simulations suggested that PLASIM-GENIE would likely require a  
390 moisture flux adjustment and *APM* was introduced as an ensemble variable. *APM*  
391 is varied across ensemble members by a linear scaling preserving the ratio of  
392 fluxes between latitude bands.

393

394 An exploratory simulation with a flux adjustment of 0.32Sv was performed and  
395 integrated net input freshwater fluxes (precipitation, evaporation, runoff and the  
396 flux adjustment) were diagnosed for the Arctic/Atlantic and the Pacific. In both  
397 basins, grid cells north of 32°S were included, following the observational  
398 estimates of Talley (2008). Values of -0.5Sv and +0.1Sv respectively were  
399 diagnosed, compared to observations of  $-0.28 \pm 0.04$  and  $+0.04 \pm 0.09$ Sv (Talley  
400 2008). Informed by this result, we allowed *APM* to vary in the range 0 to 0.32Sv.

401

402 PLASIM has also been coupled to the UVic Earth system model, creating the  
403 OSUVic model (Schmittner et al, 2010). The most significant difference between  
404 PLASIM-GENIE and USOVic is the differing complexity of the ocean models; USO-  
405 Vic incorporates the more complex primitive-equation Modular Ocean Model  
406 (MOM) version 2.2 (Pacanowski 1995) at a horizontal resolution of  $1.8^\circ \times 3.6^\circ$ ;  
407 the primitive equations include momentum advection terms neglected in our  
408 system. At T21 atmospheric resolution, the integrated Atlantic surface moisture  
409 balance simulated by OSUVic (-0.33Sv) is in good agreement with observations  
410 without any flux adjustment. However, OSUVic nevertheless simulates a weak  
411 (9Sv) Atlantic overturning circulation at T21 resolution. This was attributed in  
412 part to errors in the latitudinal distribution of the simulated moisture flux, which  
413 create low surface ocean salinities at high latitudes in the Atlantic (balanced by  
414 high salinity at low latitudes). We note that an exploratory PLASIM-GENIE  
415 simulation with a *uniformly* distributed 0.32Sv moisture flux adjustment also  
416 exhibited low Atlantic salinity at high latitudes and weak overturning.

417

#### 418 **4.1.2 SCF**

419 *SCF* scales the surface wind stresses that are applied to GOLDSTEIN. The scaling  
420 is needed because the frictional-geostrophic ocean dissipates wind energy so  
421 that increased surface wind strengths are required to compensate and drive a  
422 reasonable circulation. The conventional ensemble range for the *SCF* parameter  
423 in GENIE-1 (forced by observed climatological wind stress) is 1 to 3 (Edwards  
424 and Marsh, 2005).

425

426 In the OSUVic model (Schmittner et al 2010), the weak overturning circulation at  
427 T21 resolution discussed in Section 4.1.1 was, in addition to errors in the surface  
428 salinity distribution, partly attributed to low zonal wind-stress in the Southern  
429 Ocean, likely due to inadequate meridional resolution (c.f. Held and Phillipps,  
430 1993). In anticipation of systematically understated Southern Ocean zonal wind  
431 stress in our T21 coupling, we here allowed *SCF* to vary in the range 2 to 4.

432

#### 433 **4.2 Ensemble outputs**

434 Thirty-seven of the 50 ensemble members successfully completed the 1,000-year  
435 preindustrial spin up simulations. These simulations exhibited a global average  
436 surface air temperature of  $12.1 \pm 1.2^\circ\text{C}$  ( $1\sigma$ ). Simulation-failure was invariably  
437 associated with low frictional drag (high *ADRAG*); low frictional drag leads to  
438 unrealistically strong flow near the Equator and topographic features (Edwards  
439 and Marsh, 2005). Three successfully completed simulations (with inverse  
440 frictional drag 4.01, 3.21 and 3.98 days<sup>-1</sup>) were excluded from the ensemble on  
441 account of unreasonably strong Pacific overturning (277, -174 and 633Sv  
442 respectively). We briefly summarise some of the characteristics of the remaining  
443 thirty-four simulations in terms of their response to *APM*, *SCF* and *ADRAG*, the  
444 three parameters that dominate the ensemble variability.

445

#### 446 **4.2.1 APM**

447 The Atlantic overturning cell collapsed in all 20 simulations with *APM* less than  
448 0.16Sv. It collapsed in only five of the 14 simulations with *APM* greater than  
449 0.16Sv.

450

451 A regression of ensemble outputs suggests that the observed integrated Atlantic  
452 freshwater balance (correlation -0.88) is best reproduced for *APM* of  
453 approximately 0.13Sv, while the integrated Pacific freshwater balance  
454 (correlation +0.57) is best reproduced for *APM* of approximately 0.28Sv. Values  
455 between these limits ( $\sim 0.13$  to 0.28Sv) are therefore favoured to optimise the  
456 surface ocean inter-basin salinity distribution.

457

458 It is worth noting that these conclusions only pertain to the specific model setup  
459 considered (i.e. the vector of all *fixed* parameters). We cannot rule out the  
460 possibility that alternative model parameterisations can reproduce observed  
461 salinity and circulation fields without a moisture flux adjustment.

462

463 **4.2.2 SCF and ADRAG:** Wind stress scaling and inverse frictional drag affect the  
464 simulations in similar ways, as expected because the role of wind-stress scaling  
465 is to compensate for frictional dissipation. Many clear relationships between  
466 these parameters and simulated outputs are apparent, for instance high values of

467 either tend to strengthen overturning circulation and decrease sea-ice coverage  
468 in both hemispheres. It is interesting to note a strong negative correlation (-0.62)  
469 between *ADRAG* and the integrated surface Pacific freshwater flux, opposing a  
470 positive correlation (+0.77) with the integrated freshwater flux of the Indian  
471 Ocean. (Similar, though weaker, relationships exist with *SCF*).

472

### 473 **4.3 Selection of a ‘subjectively’ tuned parameter set**

474 Three of the 37 completed 1,000-year simulations have already been ruled out  
475 for unreasonably strong Pacific overturning and a further twenty-five because  
476 the Atlantic overturning circulation had collapsed. Two further simulations were  
477 ruled out for unacceptably low (and still cooling) global surface air temperature  
478 ( $<10^{\circ}\text{C}$ ) and two for an excessively evaporative Atlantic basin ( $\sim 0.5\text{Sv}$ , forced by  
479 *APM*  $\sim 0.3\text{Sv}$ ). The remaining five simulations were spun on for an additional  
480 1,000 years. After this spin on, two of these simulations were ruled out under a  
481 stricter global surface air temperature constraint (requiring  $>12^{\circ}\text{C}$ ), a third  
482 simulation did not exhibit penetration of Antarctic Bottom Water into the  
483 Atlantic and a fourth simulation displayed a positive Pacific overturning cell that  
484 penetrated to the ocean floor north of  $15^{\circ}\text{N}$ . The remaining simulation was  
485 clearly preferable on the basis of these simple large-scale constraints, testing for  
486 reasonable surface-ocean forcing and circulation. This ‘subjective’ parameter set  
487 (see Table 1) is therefore taken as our preferred tuning<sup>5</sup>.

488

### 489 **5.0 Simulated climate of the subjective tuning**

490 The simulated climate metrics of the subjective tuning are global average surface  
491 air temperature  $12.9^{\circ}\text{C}$ , surface Atlantic freshwater balance  $-0.34\text{Sv}$  (including  
492 the  $-0.21\text{Sv}$  moisture flux adjustment), maximum Atlantic overturning (below  
493 500m)  $15.5\text{Sv}$ , minimum Atlantic overturning  $-3.4\text{Sv}$ , and maximum Pacific

---

<sup>5</sup> We note that after the tuning ensemble was performed, the “surfstep” PLASIM subroutine was moved to the start of the diabatic time step (in the stand-alone model, PLASIM surface conditions are updated after the calculation of diabatic processes). This change was made so that boundary conditions are immediately updated after a call to GOLDSTEIN. Differences in simulated outputs were not distinguishable from internal variability.



494 overturning 8.8Sv (restricted to high latitudes and intermediate depths, see  
495 Figure 6). We now evaluate the climate in some detail.

496

497 Table 2 compares the subjectively tuned PLASIM-ENTS preindustrial global  
498 energy balance against a range of observationally constrained (present day)  
499 estimates presented in Trenberth et al (2009). Simulated fluxes are generally  
500 within the ranges of these estimates besides reflecting the simulated cold bias  
501 that is most clearly apparent in OLR (and only partially attributable to  
502 anthropogenic forcing). Although within ranges, these data suggest that too little  
503 solar radiation is absorbed within the atmosphere and too much is reflected by  
504 the surface (likely due to the high ocean albedo, Section 4.1).

505

506 Table 3 compares the simulated surface ocean net moisture fluxes in each basin  
507 with the estimates of Talley (2008). The good agreement in the Atlantic is  
508 imposed by the moisture flux adjustment. We emphasise that the requirement  
509 for a flux adjustment in this parameterisation does not necessarily indicate an  
510 inherent structural weakness in the model, pending a full exploration of  
511 parameter-space (c.f. Williamson et al 2015). The largest disagreement between  
512 these observations and the subjective tuning is the moisture flux differential  
513 between the Indian and Pacific Oceans. The global aggregates of precipitation,  
514 evaporation and runoff are in good agreement with the observationally  
515 constrained estimates of Trenberth et al (2007), with a modest low bias that is  
516 consistent with the simulated cold bias.

517

518 Figures 2 to 4 compare a selection of PLASIM-GENIE outputs against  
519 NCEP/NCAR reanalysis fields (Kalnay et al 1996). In each case we compare fifty-  
520 year PLASIM-GENIE averages of southern summer (JJA) and northern summer  
521 (DJF) with the corresponding long-term means (1981-2010) of the reanalysis  
522 data. The plotted outputs were chosen to highlight feedbacks that are neglected  
523 by the EBM, viz. 3D dynamical atmospheric transport, providing greatly  
524 improved precipitation fields and dynamic surface winds (an imposed forcing in  
525 GENIE-1), and interactive clouds (also an imposed forcing field in GENIE-1,  
526 comprising a spatiotemporal cloud albedo field and uniform OLR adjustment.)

527

528 Surface air temperature and precipitation fields are plotted in Figure 2. The cold  
529 bias of the subjective tuning is especially apparent in the high Arctic winter.  
530 Despite the global cold bias, surface air temperatures are warm-biased over the  
531 Southern Ocean, consistent with an underestimation of southern sea-ice  
532 coverage that was apparent over the entire ensemble. PLASIM precipitation  
533 fields are reasonable given our low resolution. Distinct arid regions are captured,  
534 as is the seasonal migration of the Inter-Tropical Convergence Zone and  
535 associated monsoon systems.

536

537 Figure 3 compares the surface wind fields of the subjective tuning with 10m  
538 reanalysis winds. The simulated spatiotemporal distributions are in good  
539 agreement with reanalysis, although Antarctic circumpolar wind speed is  
540 somewhat understated and too northerly (c.f. Schmittner et al 2010). We note  
541 that simulated wind speeds are at the 0.983 sigma pressure level, typically  
542  $\sim 136\text{m}$  above the surface, so that boundary layer damping is weaker than the  
543 10m reanalysis winds. Therefore we expect greater wind speeds in the PLASIM-  
544 GENIE plots, as is generally the case. Our focus here is on the wind-stress  
545 coupling and the tuned ocean state. The 3D atmospheric circulation is also  
546 reasonable. To illustrate, the simulated Southern/Northern hemisphere winter  
547 zonal wind jets ( $\sim 44/43 \text{ ms}^{-1}$ ,  $35^{\circ}\text{S}/35^{\circ}\text{N}$ , 150mbar) compare to reanalysis data  
548 ( $\sim 41/44 \text{ ms}^{-1}$ ,  $30^{\circ}\text{S}/30^{\circ}\text{N}$ , 200mbar).

549

550 Figure 4 compares incoming solar and thermal radiation fields with the  
551 reanalysis data. These fields are also chosen to reflect dynamics that are absent  
552 from GENIE-1, which applies prescribed planetary albedo fields and a globally  
553 uniform OLR adjustment to represent the effect of clouds on the radiation  
554 balance. The outputs plotted in Figures 3 and 4 were chosen to focus on  
555 dynamics that are entirely absent from GENIE-1: interactive winds and  
556 interactive clouds. While the inclusion of these dynamics is not expected to  
557 improve the simulated climatology (i.e. when compared to simulations that are  
558 forced with climatological fields), their inclusion represents a substantial

559 upgrade through the capture of important Earth system feedbacks neglected in  
560 GENIE-1.

561

562 An important example of substantial improvement over the climatology of  
563 GENIE-1 is atmospheric moisture transport, previously touched upon in the  
564 context of Figure 2. Figure 5 compares PLASIM-GENIE vegetative carbon (5a)  
565 and GENIE-1 vegetation carbon (5b, data reproduced from Holden et al, 2013a,  
566 Fig 1a) and highlights various aspects of the improved moisture transport. In  
567 GENIE-1, deserts are poorly resolved (too moist) and boreal forest does not  
568 penetrate far into the continental interior of Eurasia (too dry); these are both  
569 shortcomings that arise from diffusive moisture transport (Lenton et al 2006).  
570 Although the deserts of the Southern hemisphere are not well resolved in either  
571 model, the larger deserts of the Northern hemisphere are distinct in PLASIM-  
572 GENIE, while simulated boreal forest penetrates the Eurasian interior. Global  
573 terrestrial carbon storage in the subjective tuning of PLASIM-GENIE is 604GTC  
574 (vegetation) and 1,971GTC (soil). These compare to 491-574 GTC and 1,367-  
575 1,416GTC respectively in GENIE-1 (Lenton et al 2006). The significantly higher  
576 soil carbon values in PLASIM-GENIE primarily reflect the increased area of  
577 Eurasian boreal forest, where soil carbon is respired slowly due to the low  
578 temperatures. The global terrestrial carbon pools are consistent with ranges of  
579 460-660GTC (vegetation) and 850-2400GTC (soil) derived from a range of  
580 observational and modelling studies and summarised in Bondeau et al (2007).

581

582 Budyko's (1974) framework of climate analysis is based on the climate mean  
583 dryness ratio  $D$  or aridity index (mean energy supply or net radiation  $N$  to mean  
584 water supply or precipitation  $P$ ). It provides quantitative geobotanically relevant  
585 thresholds for land surface climate regimes that are related to vegetation  
586 structures (Fig. 6c): Tundra,  $D < 1/3$ , and forests,  $1/3 < D < 1$ , are energy limited  
587 ( $D < 1$ ), because available energy  $N$  is low, so that runoff exceeds evaporation for  
588 given precipitation,  $E \sim N$ . Steppe and savanna,  $1 < D < 2$ ; semi-desert,  $2 < D < 3$ ;  
589 and desert  $3 > D$ , are water-limited climates ( $D > 1$ ), where the available energy  
590 is so high that water supplied by precipitation evaporates, which then exceeds  
591 runoff,  $E - P$ . This analysis highlights the Tibetan Plateau and North American

592 Arctic climates and demonstrates consistency with the simulated vegetation  
593 carbon (Fig 6a). The similarity with ERA-interim based analysis (Cai et al 2014,  
594 Fig 1a) is notable. Similarly, a bucket model interpretation of the land surface  
595 climate (Fraedrich et al 2015) is possible using the soil moisture fraction,  
596  $S=s/s^*=E/N$ , and is plotted in Fig. 5d.

597

598 Sea-ice distributions (not illustrated) exhibit a systematic bias towards low  
599 southern sea-ice area across the ensemble, with an annual average of 2.8 million  
600 km<sup>2</sup> in the subjective tuning; this compares to observational estimates of 11.5  
601 million km<sup>2</sup> (Cavalieri et al 2003). Surface air temperature over the southern  
602 ocean is warm biased with respect to the reanalysis data, despite a modest cold  
603 bias in the global temperature (Figure 2). While this may in part be a  
604 consequence of reduced sea-ice (through the albedo feedback), the continued  
605 presence of the warm bias in southern summer suggests the possibility that the  
606 bias arises in the atmosphere. The decision to control the global temperature  
607 with *acllwr* (Section 4.1) preferentially warms cloudy regions and may have  
608 contributed. Indeed, simulated downward thermal radiation exhibits a  
609 significant **positive** bias over the Southern Ocean (Figure 4). A thorough  
610 investigation of the source of this bias is beyond the scope of this study,  
611 requiring consideration of uncertainties in atmospheric and ocean energy  
612 transport, and in solar and thermal radiative transfer, considering clouds, water  
613 vapour, and surface processes.

614

615 Figure 6 illustrates aspects of the simulated ocean state that directly reflect the  
616 constraints imposed upon the subjective parameter set and require little further  
617 discussion. It is worth emphasising again that the simulation of realistic salinity  
618 fields and ocean circulation required an Atlantic-Pacific moisture flux adjustment  
619 in this parameterisation (Sections 4.1.1 and 4.2.1).

620

621 The upper panel of Figure 7 plots the PLASIM-GENIE barotropic streamfunction.  
622 Simulated gyre strengths are 24Sv/-26Sv North/South Atlantic, 53Sv/-41Sv  
623 North/South Pacific and 5Sv/-32Sv North/South Indian Ocean. For comparison,  
624 the gyre strengths of climatological wind-forced 64x32 GENIE-1 were simulated

625 at  $\sim 20\text{Sv}/-20\text{Sv}$  North/South Atlantic,  $\sim 30\text{Sv}/-30\text{Sv}$  North/South Pacific and  
626  $\sim 3\text{Sv}/-40\text{Sv}$  North/South Indian Ocean at (Figure 19d, Marsh et al 2011).  
627 Stronger gyres in the PLASIM-GENIE simulation compared to the GENIE-1  
628 simulation are likely to be related to larger values of wind-stress scaling in the  
629 PLASIM-GENIE case, given that the simulated wind forcing is relatively close to  
630 climatology. The observed Gulf Stream strength is estimated at  $32\text{Sv}$ , while  
631 simulated strengths ranged from 13 to  $48\text{Sv}$  in the multi-model comparison of  
632 Balan-Sarojini et al (2011). The Antarctic Circumpolar Current (ACC) is weaker  
633 in PLASIM-GENIE ( $30\text{Sv}$ ) than GENIE-1 ( $47\text{Sv}$ ), presumably reflecting the weak  
634 simulated Southern Ocean zonal winds (see Figure 3). Note that both models  
635 significantly understate the ACC strength compared to observations of  $140\pm 6\text{Sv}$   
636 (Ganachaud and Wunsch, 2000).

637

638 The lower panel of Figure 7 illustrates high-frequency AMOC variability driven  
639 by atmospheric dynamics, behaviour that is absent from GENIE-1 (Balan-Sarojini  
640 et al 2011). The maximum Atlantic overturning circulation is plotted through an  
641 arbitrary year (year 100 of a spin on simulation), together with the 100-year  
642 mean and standard deviation.

643

## 644 **6.0 Summary and conclusions**

645

646 We have presented a new intermediate complexity AOGCM PLASIM-GENIE,  
647 which reproduces the main features of the climate system well and represents a  
648 substantial upgrade to GENIE-1 through the representation of important  
649 atmospheric dynamical feedbacks that are absent in an EMBM. PLASIM-GENIE  
650 has been developed to join the limited number of intermediate complexity  
651 models with primitive equation atmospheric dynamics. It supersedes an earlier  
652 coupling with the IGCM ('GENIE-2'), which was contaminated with spurious  
653 numerically generated features, limiting its usefulness.

654

655 The simple 'subjective' tuning approach applied here considered only six ocean  
656 parameters, seeking a reasonable ocean circulation when coupled to PLASIM-  
657 ENTS (both PLASIM and ENTS have previously been tuned with climatological

658 forcing). This limited tuning approach required approximately 2 CPU years,  
659 demanding but readily tractable, representing approximately two weeks of  
660 computation on 50 cluster nodes.

661

662 A reasonable ocean circulation state and salinity distribution required the  
663 application of an Atlantic-Pacific moisture flux adjustment. We do not rule out  
664 the possibility that a full investigation of PLASIM-GENIE parametric uncertainty  
665 could generate a plausible ocean circulation without a flux adjustment, and may  
666 additionally resolve the understated southern sea ice. However, a  
667 comprehensive tuning will demand the application of more complex statistical  
668 approaches designed to deal with computationally demanding simulators. For  
669 instance, the use of emulators to inform a sequential ensemble design process  
670 has been demonstrated to yield a ~100-fold reduction in computational demand  
671 (Holden et al 2015).

672

## 673 **7.0 Code availability**

674 The code base is stored on a password-protected SVN server

675 [https://svn.ggy.bris.ac.uk/subversion/genie/branches/PLASIM\\_coupling](https://svn.ggy.bris.ac.uk/subversion/genie/branches/PLASIM_coupling)

676

677 Contact the authors for the password. The model is under continuous development;  
678 see SVN revision 9697 for traceability.

679

680 We recommend setting up a root directory (e.g. PLASIM-GENIE) containing the  
681 subdirectories `genie_output` and `genie`, the latter containing the directory structure  
682 downloaded from the SVN repository.

683

684 In addition to the source code, PLASIM-GENIE makes use of several applications  
685 and packages. You must have the following list of prerequisites installed on your  
686 computer before you can run the model: Python, Perl, GNU make, the BASH shell, a  
687 C++ compiler, a Fortran compiler that supports Fortran90, and NetCDF libraries  
688 (compiled on the same computer using the same compilers that you will use to  
689 compile PLASIM-GENIE).

690

691 Before you compile the model you must provide information about i) where you have  
692 installed the source code, ii) which compilers you are using, and iii) the location of  
693 the netCDF libraries that you have created; this is achieved by editing the files  
694 **user.mak** and **user.sh** in the directory genie-main. Comments in those files explain  
695 which lines need to be edited.

696

697 A configuration file contains all the information required to specify a simulation.  
698 The code base includes a configuration file to perform a 1,000-year spin-up with the  
699 subjective parameter set "genie/genie-main/configs/pl\_go\_gs\_GMD.xml". This  
700 configuration file has been fully commented for traceability to this model description  
701 paper and to explain how to generalize to other model realisations. To run this  
702 simulation, enter the genie/genie-main directory and type:

703

704 make cleanall

705 ./genie.job -f configs/pl\_go\_gs\_GMD.xml

706

707 The outputs of this simulation will be directed to genie\_output/GMD\_subjective.

708

709 *Acknowledgements.* The work of Kirk, Lunkeit and Zhu was supported through  
710 the Cluster of Excellence 'CliSAP' (EXC177), Universität Hamburg, funded  
711 through the German Science Foundation (DFG).

712

## 713 **References**

714

715 Annan, J.D., Lunt D.J., Hargreaves, J.C. and Valdes, P.J.: Parameter estimation in an  
716 atmospheric GCM using the Ensemble Kalman Filter. *Nonlinear Processes in*  
717 *Geophysics*, European Geosciences Union (EGU), 12, 363-371, doi:1607-  
718 7946/npg/2005- 12-363, 2005.

719

720 Balan-Sarajini, B., Gregory, J. M., Tailleux, R., Bigg, G. R., Blaker, A. T., Cameron, D.  
721 R., Edwards, N. R., Megann, A. P., Shaffrey, L. C. and Sinha, B.: High frequency  
722 variability of the Atlantic meridional overturning circulation, *Ocean Sci.*, 7, 471-  
723 486, doi:10.5194/os-7-471-2011, 2011.

724

725 Betts, A.K. and Miller, M.J.: A new convective adjustment scheme. Part II: Single  
726 column tests using GATE wave, BOMEX, ATEX and arctic air-mass data sets.  
727 Quart. J. R. Met. Soc., 112, 693–709, 1986.

728

729 Bondeau, A., Smith, P. C., Zaehle, S., Schaphoff, S., Lucht, W., Cramer, W., Gerten,  
730 D., Lotze-Campen, H., Müller, C., Reichstein, M., and Smith, B.: Modelling the role  
731 of agriculture for the 20th century global terrestrial carbon balance, Glob.  
732 Change Biol., 13, 679–706, doi:10.1111/j.1365- 2486.2006.01305.x, 2007.

733

734 Budyko, M. : Climate and Life. Vol. 18, Academic Press, 508 pp, 1974.

735

736 Cai, D., Fraedrich, K., Sielmann, F., Guan, Y., Guo, S., Zhang, L. and Zhu, X.: Climate  
737 and vegetation: an ERA-interim and GIMMS NVDI analysis, Journal of Climate, 27,  
738 5111-5118, doi: 10.1175/JCLI-D-13-00674.1, 2014

739

740 Cavalieri, D. J., Parkinson, C. L., and Yinnikov, K. Y.: 30-year satellite record  
741 reveals contrasting Arctic and Antarctic decadal sea-ice variability, Geophys. Res.  
742 Lett., 30, 1970, doi:10.1029/2003GL018031, 2003.

743

744 Dahms, E., Borth, H., Lunkeit, F., and Fraedrich, K.: ITCZ splitting and the  
745 influence of large-scale eddy fields on the Tropical mean state, J. Meteorol. Soc.  
746 Jpn., 89, 399–411, doi:10.2151/jmsj.2011-501, 2011.

747

748 Edwards, N.R. and Marsh, R.: Uncertainties due to transport-parameter sensitivity in  
749 an efficient 3-D ocean-climate model, Climate Dynamics, 24, 415-433, doi:  
750 10.1007/s00382-004-0508-8, 2005.

751

752 Edwards, N.R., Willmott, A.J. and Killworth, P.D.: On the role of topography and  
753 wind stress on the stability of the thermohaline circulation. J. Physical Oceanography,  
754 28, 756-778, 1998.

755



756 Fanning, A. F. and Weaver, A. J.: An atmospheric energy-moisture balance model:  
757 climatology, interpentadal climate change, and coupling to an ocean general  
758 circulation model, *Journal of Geophysical Research*, 101, 15111–15128,  
759 doi:10.1029/96JD01017, 1996.  
760

761 de Forster, P.M., Blackburn, M., Glover, R. and Shine, K.P.: An examination of  
762 climate sensitivity for idealised climate change experiments in an intermediate  
763 general circulation model. *Climate Dynamics*, 16, 833–849, doi:  
764 10.1007/s003820000083, 2000.  
765

766 Fraedrich, K., Kirk, E., Luksch, U. and Lunkeit, F.: The portable university model of  
767 the atmosphere (PUMA): Storm track dynamics and low-frequency variability,  
768 *Meteorologische Zeitschrift*, 14, 735-745, doi: 10.1127/0941-2948/2005/0074, 2005.  
769

770 Fraedrich, K. and Lunkeit, F.: Diagnosing the entropy budget of a climate model,  
771 *Tellus A*, 60, 921–931, doi:10.1111/j.1600- 0870.2008.00338.x, 2008, 2008.  
772

773 Fraedrich, K.: A suite of user-friendly climate models: Hysteresis experiments,  
774 *The European Physical Journal Plus*, 127, 10.1140/epjp/i2012-12053-7, 2012  
775

776 Fraedrich, K., Sielmann, F., Cai, D., and Zhu, X.: Climate dynamics on watershed  
777 scale: along the rainfall-runoff chain. In: *The Fluid Dynamics of Climate*,  
778 International Centre for Mechanical Sciences (CISM), Springer Verlag, 183-209,  
779 2016.  
780

781 Frierson, D.M.W., Held, I.M. and Zurita-Gotor, P.: A gray-radiation aquaplanet  
782 moist GCM. Part I. Static stability and eddy scale, *J. Atmos. Sci.*, 63, 2548-2566,  
783 2006  
784

785 Held, I.M. and Phillipps, P.J.: Sensitivity of the eddy momentum flux to meridional  
786 resolution in atmospheric GCMs, *Journal of Climate*, 6, 499-507, 1995.  
787

788 Hibler W.D.: Dynamic thermodynamic sea ice model, *J Phys Oceanogr*, 9, 815–  
789 846, 1979.  
790

791 Holden, P.B. and Edwards, N.R.: Dimensionally reduced emulation of an AOGCM  
792 for application to integrated assessment modelling, *Geophysical Research*  
793 *Letters*, 37, L21707, doi:10.1029/2010GL045137, 2010.  
794

795 Holden, P.B., Edwards, N.R., Oliver, K.I.C, Lenton, T.M. and Wilkinson R.D.: A  
796 probabilistic calibration of climate sensitivity and terrestrial carbon storage in  
797 GENIE-1, *Climate Dynamics*, 35, 785-908, doi: 10.1007/s00382-009-0630-8,  
798 2010.  
799

800 Holden, P.B., Edwards, N.R., Gerten, D. and Schaphoff, S.: A model-based constraint  
801 on CO<sub>2</sub> fertilisation, *Biogeosciences*, 10, 339-355, doi:10.5194/bg-10-339-2013,  
802 2013a.  
803

804 Holden, P.B., Edwards, N.R., Müller, S.A., Oliver, K.I.C., Death, R.M. and Ridgwell,  
805 A.: Controls on the spatial distribution of  $\delta^{13}\text{C}$ , *Biogeosciences*, 10, 1815-1833,  
806 doi:10.5194/bg-10-1815-2013, 2013b.  
807

808 Holden, P.B., Edwards, N.R., Garthwaite, P.H., Fraedrich, K., Lunkeit, F., Kirk, E.,  
809 Labriet, M., Kanudia, A. and Babonneau, F.: PLASIM-ENTSem v1.0: a spatio-  
810 temporal emulator of future climate change for impacts assessment, *Geosci.*  
811 *Model Dev.*, 7, 433–451, doi:10.5194/gmd-7-433-2014, 2014.  
812

813 Holden, P.B., Edwards, N.R., Hensman, J. and Wilkinson, R.D.: ABC for climate:  
814 dealing with expensive simulators, In S. A. Sisson, Y. Fan, and M. Beaumont eds.  
815 *Approximate Bayesian Computation: Likelihood-Free Methods for Complex Models*,  
816 Chapman and Hall, in press.  
817

818 Hoskins, B.J. and Simmons, A.J.: A multi-layer spectral model and the semi-  
819 implicit method, *Quart. J. R. Met. Soc.*, 101, 637-655, doi: 10.1002/  
820 qj.49710142918, 1975.

821

822 Kalnay, E., Kanamitsu, M., Kistler, R., Collins, W., Deaven, D., Gandin, L., Iredell, M.,  
823 Saha, S., White, G., Woollen, J., Zhu, Y., Leetmaa, A., Reynolds, R., Chelliah, M.,  
824 Ebisuzaki, W., Higgins, W., Janowiak, J., Mo, K. C., Ropelewski, C., Wang, J., Jenne,  
825 R., and Joseph, D.: The NCEP/NCAR 40-Year Reanalysis Project. *Bull. Amer.*  
826 *Meteor. Soc.*, **77**, 437–471, 1996.

827

828 Labriet, M., Joshi, S.R., Vielle, M., Holden, P.B., Edwards, N.R., Kanudia, A.,  
829 Loulou, R. and Babonneau, F.: Worldwide impacts of climate change on energy for  
830 heating and cooling, *Mitigation and Adaptation Strategies for Global Change*, doi:  
831 10.1007/s11027-013-9522-7, 2013.

832

833 Lenton, T.M., Williamson, M.S., Edwards, N.R., Marsh, R., Price, A.R., Ridgwell, A.J.,  
834 Shepherd, J.G., Cox, S.J. and The GENIE team: Millennial timescale carbon cycle  
835 and climate change in an Efficient Earth system model, *Climate Dynamics*, **26**,  
836 687-711, doi: 10.1007/s00382-006-0109-9, 2006.

837

838 Lenton, T. M., Aksenov, Y., Cox, S.J., Hargreaves, J.C., Marsh, R., Price, A.R., Lunt,  
839 D.J., Annan, J.D., Cooper-Chadwick, T., Edwards, N.R., S. Goswami, S., Livina,  
840 V.N., P. J. Valdes, P.J., Yool, A., Harris, P.P., Jiao, Z., Payne, A.J., Rutt, I.C.,  
841 Shepherd, J.G. Williams, G., Williamson, M.S.: Effects of atmospheric dynamics and  
842 ocean resolution on bi-stability of the thermohaline circulation examined using the  
843 Grid Enabled Integrated Earth system modelling (GENIE) framework, *Climate*  
844 *Dynamics*, **29**, 591–613, doi:10.1007/s00382-007-0254-9, 2007.

845

846 Lunkeit, F., Böttinger, M., Fraedrich, K., Jansen, H., Kirk, E., Kleidon, A. and Luksch  
847 U.: Planet Simulator Reference Manual Version 15.0,  
848 <http://epic.awi.de/29588/1/Lun2007d.pdf>, 2007.

849

850 Kleidon, A., Fraedrich, K., and Low, C.: Multiple steady-states in the terrestrial  
851 atmosphere-biosphere system: a result of a discrete vegetation classification?,  
852 *Biogeosciences*, **4**, 707–714, doi:10.5194/bg-4-707-2007, 2007.

853

854 Kuo, H. L.: On formation and intensification of tropical cyclones through latent heat  
855 release by cumulus convection. *J. Atmos. Sci.*, 22, 40–63, 1965.

856

857 Kuo, H. L.: Further studies of the parameterization of the influence of cumulus  
858 convection on large-scale flow. *J. Atmos. Sci.*, 31, 1232–1240, 1974.

859

860 Marsh, R., Müller, S.A., Yool, A. and Edwards, N.R.: Incorporation of the C-  
861 GOLDSTEIN efficient climate model into the GENIE framework: “eb-go-gs”  
862 configurations of GENIE, *Geosci. Model Dev.*, 4, 957-992, doi:10.5194/gmd-4-957-  
863 2011, 2011.

864

865 Matthews, H.D. and Caldeira, K.: Transient climate-carbon simulations of planetary  
866 geoengineering, *PNAS*, 104, 9949–9954, doi:10.1073/pnas.0700419104, 2007.

867

868 Mercure, J.-F., Pollitt, H., Chewpreecha, U., Salas, P., Foley, A.M., Holden, P.B. and  
869 Edwards, N.R.: The dynamics of technology diffusion and the impacts of climate  
870 policy instruments in the decarbonisation of the global electricity sector, *Energy*  
871 *Policy*, 73, 686-700, doi:10.1016/j.enpol.2014.06.029, 2014.

872

873 Micheels, A. and Montenari, M.: A snowball Earth versus a slush-ball Earth:  
874 Results from Neoproterozoic climate modeling sensitivity experiments,  
875 *Geosphere*, 4, 401–410, doi: 10.1130/GES00098.1, 2008.

876

877 Molteni, F.: Atmospheric simulations using a GCM with simplified physical  
878 parameterizations. I: Model climatology and variability in multi-decadal  
879 experiments, *Climate Dynamics*, 20, 175–191, 2003.

880

881 Oliver, K. I. C. and Edwards, N. R.: Location of potential energy sources and the  
882 export of dense water from the Atlantic Ocean, *Geophys. Res. Lett.*, 35, L22604,  
883 doi:10.1029/2008GL035537, 2008.

884

885 Oort, A.H.: Global atmospheric circulation statistics, 1958– 1973:NOAA Prof Pap  
886 14, 1983.

887

888 Pacanowski, R.: MOM 2 Documentation User's Guide and Reference Manual,  
889 GFDL Ocean Group Technical Report. NOAA, GFDL. Princeton, 232pp, 1995.

890

891 Plattner, G.-K., R. Knutti, F. Joos, T. F. Stocker, W. von Bloh, V. Brovkin, D.  
892 Cameron, E. Driesschaert, S. Dutkiewicz, M. Eby, N. R. Edwards, T. Fichefet, J. C.  
893 Hargreaves, C. D. Jones, M. F. Loutre, H. D. Matthews, A. Mouchet, S. A. Mueller, S.  
894 Nawrath, A. Price, A. Sokolov, K. M. Strassmann, and A. J. Weaver 2008 Long-term  
895 climate commitments projected with climate - carbon cycle models. Journal of  
896 Climate, Vol. 21, pp. 2721-2751, doi: 10.1175/2007JCLI1905.1, 2008

897

898 Roscher, M., Stordal, F., and Svenson, H.: The effect of global warming and global  
899 cooling on the distribution of the latest Permian climate zones, Palaeogeogr.  
900 Palaeocl., 309, 186–200, doi:10.1016/j.palaeo.2011.05.042, 2011.

901

902 Sarojini, B.B., Gregory, J.M., Tailleuc, R., Bigg, G.R., Blaker, A.T., Cameron, D.R.,  
903 Edwards, N.R., Megann, A.P., Shaffrey, L.C. and Sinha, B.: High frequency  
904 variability of the Atlantic meridional overturning circulation, Ocean Science, 7, 471-  
905 486, doi:10.5194/os-7-471-2011, 2011.

906

907 Schmittner, A., Silva, T.A.M., Fraedrich, K., Kirk, E. and Lunkeit, F.: Effects of  
908 mountains and ice sheets on global ocean circulation, Journal of Climate, 24, 2814-  
909 2829, DOI: 10.1175/2010JCLI3982.1, 2010.

910

911 Semtner, A.J.: Model for thermodynamic growth of sea ice in numerical  
912 investigations of climate, J Phys Oceanogr, 6, 379–389, 1976.

913

914 Severijns, C.A. and Hazeleger, W.: The efficient global primitive equation climate  
915 model SPEEDO V2.0, Geosci. Model Dev., 3, 105-122, [www.geosci-model-](http://www.geosci-model-dev.net/3/105.2010/)  
916 [dev.net/3/105.2010/](http://www.geosci-model-dev.net/3/105.2010/), 2010.

917

918 Slingo, A., and Slingo, J.M.: Response of the National Center for Atmospheric  
919 Research community climate model to improvements in the representation of clouds.  
920 *J. Geoph. Res.*, 96, 341-357, 1991.  
921

922 Talley, L.D.: Freshwater transport estimates and the global overturning circulation:  
923 Shallow, deep and throughflow components, *Progress in Oceanography*, 78, 257-303,  
924 doi:10.1016/j.pocean.2008.05.001, 2008.  
925

926 Trenberth, K.E., Smith, L., Qian, T., Dai, A. and Fasullo, J.: Estimates of the global  
927 water budget and its annual cycle using observational and model data, *Journal of*  
928 *Hydrometeorology – Special Section*, 8, 758-769, doi: 10.1175/JHM600.1, 2007.  
929

930 Trenberth, K.E., Fasullo, J.T. and Kiehl, J.: Earth's global energy budget, *Bulletin of*  
931 *the American Meteorological society*, 90, 311-323, doi:10.1175/2008BAMS2634.1,  
932 2009.  
933

934 Williams, J.H.T., Smith, R.S., Valdes, P.J., Booth, B.B.B. and Osprey, A.: Optimising  
935 the FAMOUS climate model: inclusion of global carbon cycling, *Geosci. Model Dev.*,  
936 6, 141-160, doi: 10.5194/gmd-6-141-2013, 2013.  
937

938 Williamson, D., Blaker, A.T., Hampton, C. and Salter, J.: Identifying and removing  
939 structural biases in climate models with history matching, *Climate Dynamics*, 45,  
940 1299-1324, doi: 10.1007/s00382-014-2378-z, 2015.  
941

942 Williamson, M.S., Lenton, T.M., Shepherd, J.G. and Edwards, N.R.: An efficient  
943 numerical terrestrial scheme (ENTS) for Earth system modelling, *Ecological*  
944 *modelling*, 198, 362-374, doi:10.1016/j.ecolmodel.2006.05.027, 2006.  
945

946 Zickfeld, K., Eby, M., Weaver, A. J., Crespin, E., Fichet, T., Goosse, H., Philippon-  
947 Berthier, G., Edwards, N. R., Holden, P. B., Eliseev, A. V., Mokhov, I. I., Feulner, G.,  
948 Kienert, H., Perrette, M., Schneider von Deimling, T., Forest, C. E., Joos, F., Spahni,  
949 R., Steinacher, M., Kawamiya, M., Tachiiri, K., Kicklighter, D., Monier, E.,  
950 Schlosser, A., Sokolov, A. P., Matsumoto, K., Tokos, K., Olsen, S. M., Pedersen, J.  
951 O. P., Shaffer, G., Ridgwell, A., Zeng, N., and Zhao, F.: Long-term climate change

952 commitment and reversibility, *J. Climate*, 26, 5782-5809, doi: 10.1175/JCLI-D-12-  
953 00584.1, 2013.  
954  
955

956 **TABLES**

Parameter	Description	Range	Subjective tuning
APM (Sv)	Atlantic-Pacific moisture flux adjustment	0 to 0.32	0.2132
OVD (m <sup>2</sup> s <sup>-1</sup> )	Reference diapycnal diffusivity	2x10 <sup>-5</sup> to 2x10 <sup>-4</sup>	1.583x10 <sup>-4</sup>
OHD (m <sup>2</sup> s <sup>-1</sup> )	Isopycnal diffusivity	500 to 5,000	1,937
SCF (dimensionless)	Wind stress scaling	2 to 4	3.788
ADRAG (days)	Inverse ocean drag	0.5 to 5.0	2.069
OP1 (dimensionless)	Power law for diapycnal diffusivity depth profile	0.5 to 1.5	0.8200

957 **Table 1:** Ensemble varied parameters.

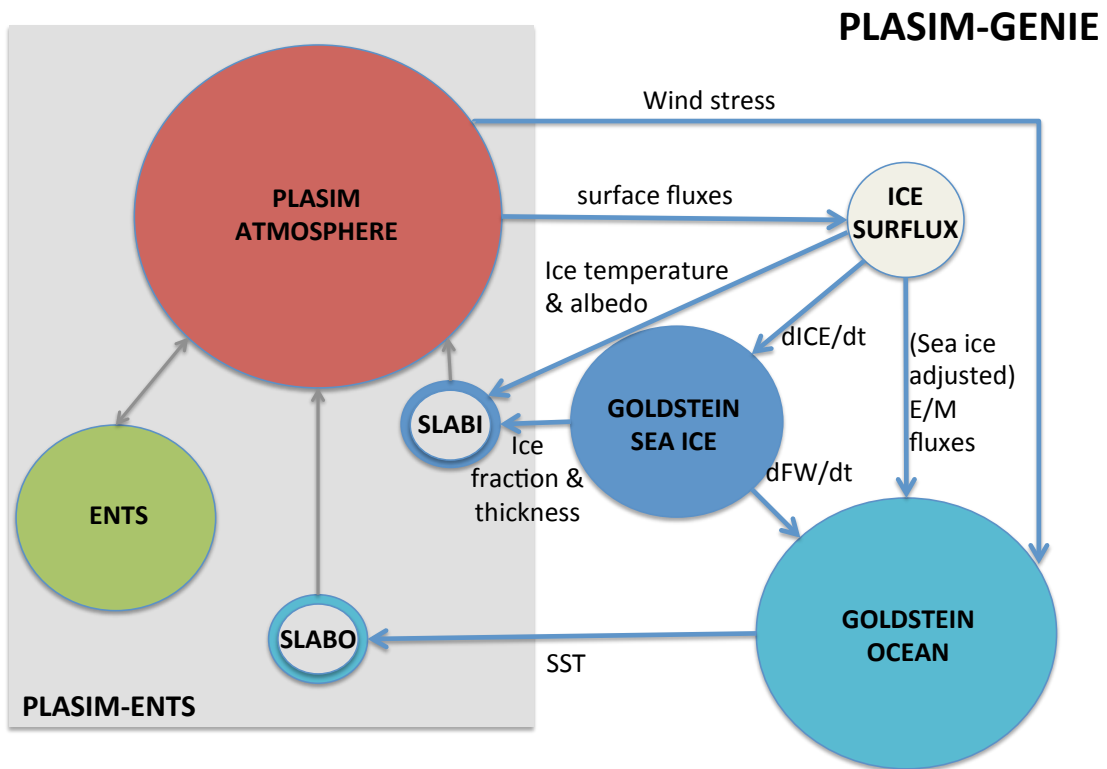
Solar radiation (Wm <sup>-2</sup> )					
	Incoming TOA	Reflected by atmosphere	Absorbed by atmosphere	Reflected by surface	Absorbed by surface
PLASIM-GENIE	341	75	66	39	161
ERBE (1985-1989)	339-343	70-83	64-81	23-45	156-169
CERES (2000-2004)	339-342	69-82	64-78	23-45	161-170
Planetary radiation and heat fluxes (Wm <sup>-2</sup> )					
	Sensible heat	Latent heat	Back radiation	Upward surface radiation	Outgoing radiation OLR
PLASIM-GENIE	20	78	323	386	228
ERBE (1985-1989)	15-24	78-85	324-345	390-396	235-254
CERES (2000-2004)	15-19	83-90	324-345	394-397	236-254

958 **Table 2:** The global energy balance of subjectively-tuned PLASIM-GENIE in the  
 959 preindustrial state compared against estimates derived from the 'Earth Radiation  
 960 Budget Experiment' ERBE (1985-1989), when the Earth's radiation balance was in  
 961 approximate equilibrium, and the 'Clouds and Earth's Radiant Energy System'  
 962 CERES data (2000-2004). The observational uncertainties reflect a range of  
 963 analyses summarised in Trenberth et al (2009).

Surface ocean moisture fluxes (Sv)						
	Atlantic/Arctic Ocean	Pacific Ocean	Indian Ocean	Southern Ocean	Total Ocean	Trenberth et al (2007)
Precipitation	1.96	4.76	1.67	2.89	<b>11.28</b>	11.8
Evaporation	-2.68	-5.48	-1.98	-2.52	<b>-12.66</b>	-13.1
Run off	0.59	0.36	0.23	0.18	<b>1.37</b>	1.3
Flux adjustment	-0.21	0.21	0.00	0.00	<b>0.00</b>	
<b>Net</b>	<b>-0.34</b>	<b>-0.14</b>	<b>-0.07</b>	<b>0.56</b>	<b>0.00</b>	
Talley (2008)	-0.28±0.04	0.04±0.09	-0.37±0.10	0.61±0.13		

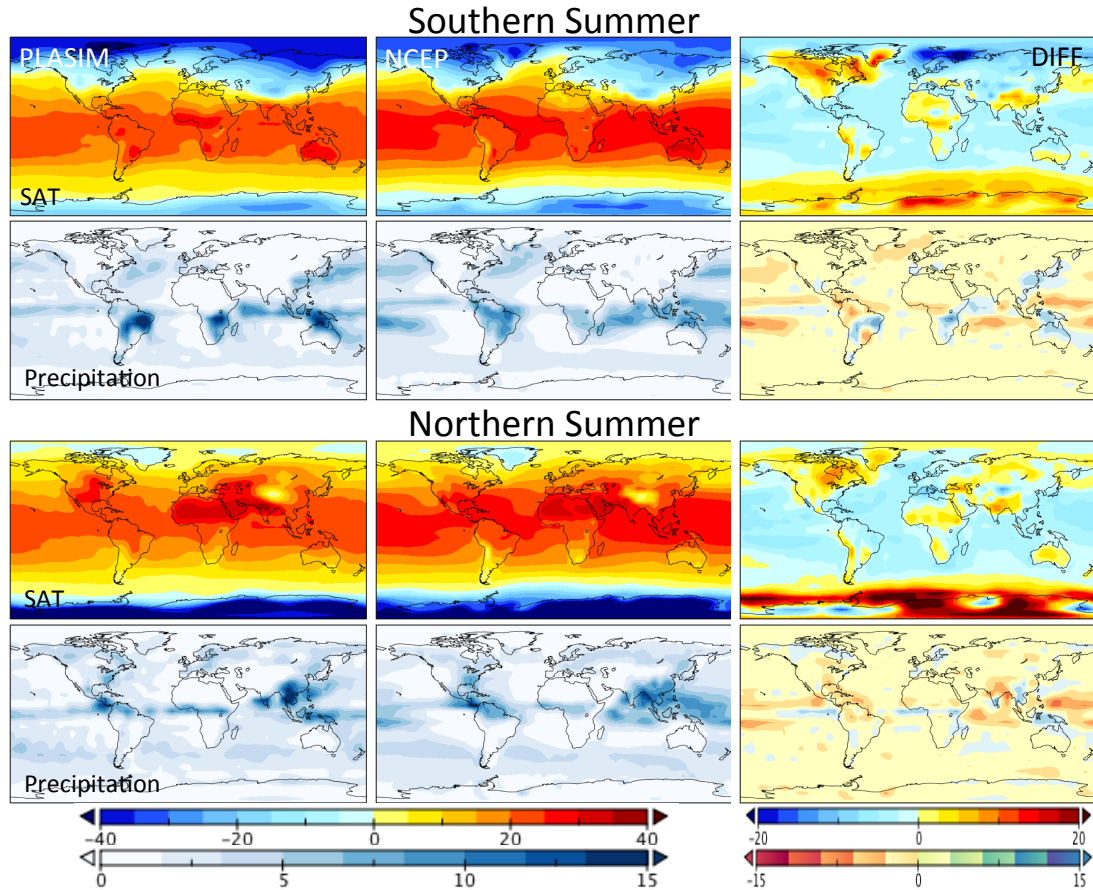
964 **Table 3:** Simulated surface ocean moisture fluxes of the subjective tuning and  
 965 observationally constrained estimates. The definition of ocean basin boundaries  
 966 follows Talley (2008) viz. Atlantic and Indian Oceans north of 32°S, Pacific Ocean  
 967 north of 28°S.





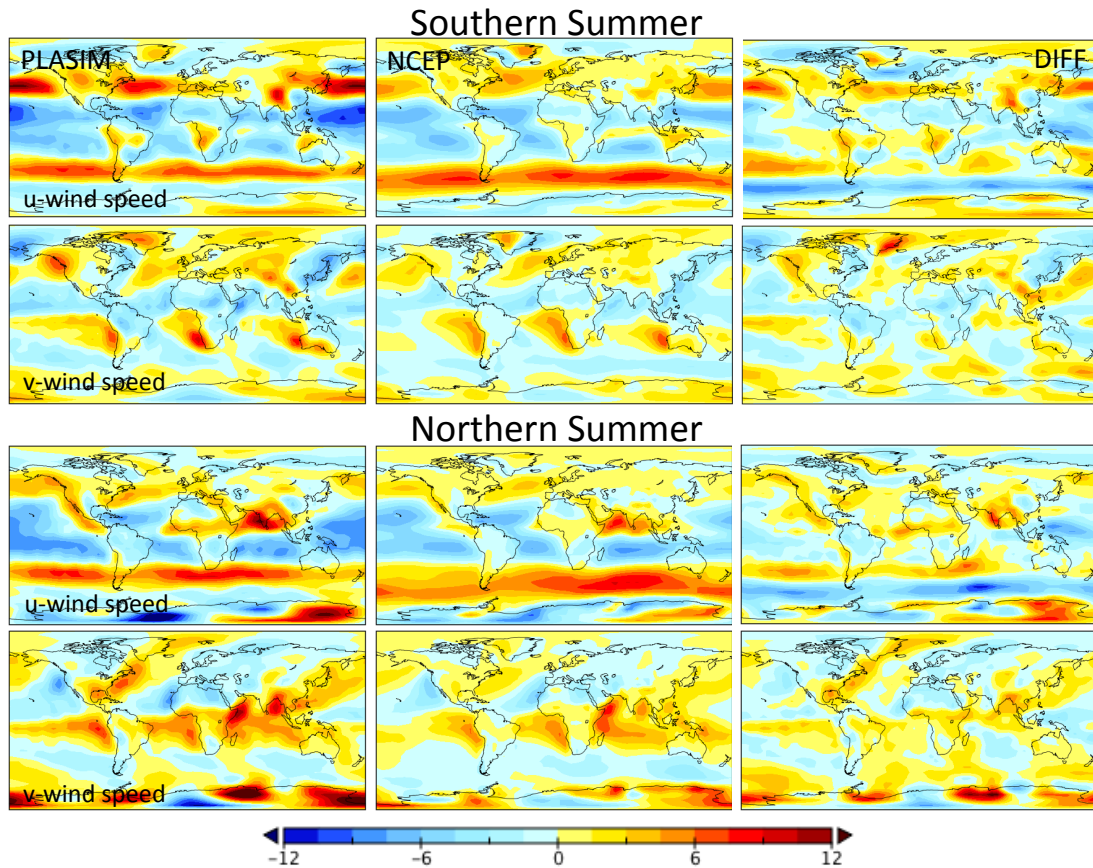
969  
 970  
 971  
 972  
 973  
 974  
 975  
 976  
 977  
 978  
 979  
 980

**Figure 1:** A schematic of the PLASIM-GENIE coupling. The circles represent the component modules, with sizes indicative of their relative complexity. The grey box defines the PLASIM-ENTS model, which has been retained in its entirety; hollow circles (SLABO and SLABI) are dummy PLASIM modules, retained only to specify ocean and sea-ice boundary conditions from GOLDSTEIN outputs; grey lines are energy and moisture fluxes that are calculated within the pre-existing PLASIM-ENTS coupling. Blue arrows are variables passed in the PLASIM-GENIE coupling. ICE-SURFLUX is the new surface flux routine that was developed for the coupling (see Section 3.3)



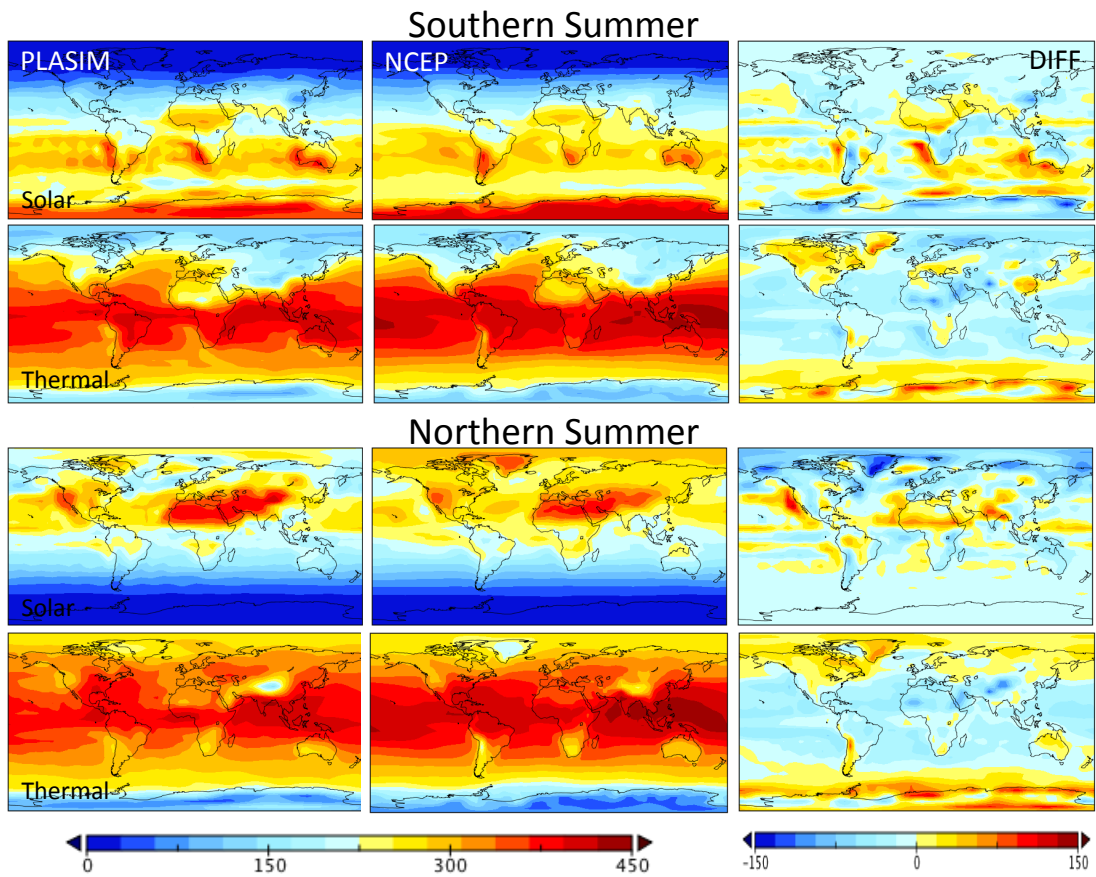
981  
 982  
 983  
 984  
 985  
 986

**Figure 2:** Seasonal surface air temperature ( $^{\circ}\text{C}$ ) and precipitation (mm/day). Left: PLASIM-GENIE 50-year average. Centre: long-term average (1981-2010) NCEP/NCAR reanalysis fields (Kalnay et al 1996). Right: difference (PLASIM-NCEP).



987  
 988  
 989  
 990  
 991  
 992  
 993

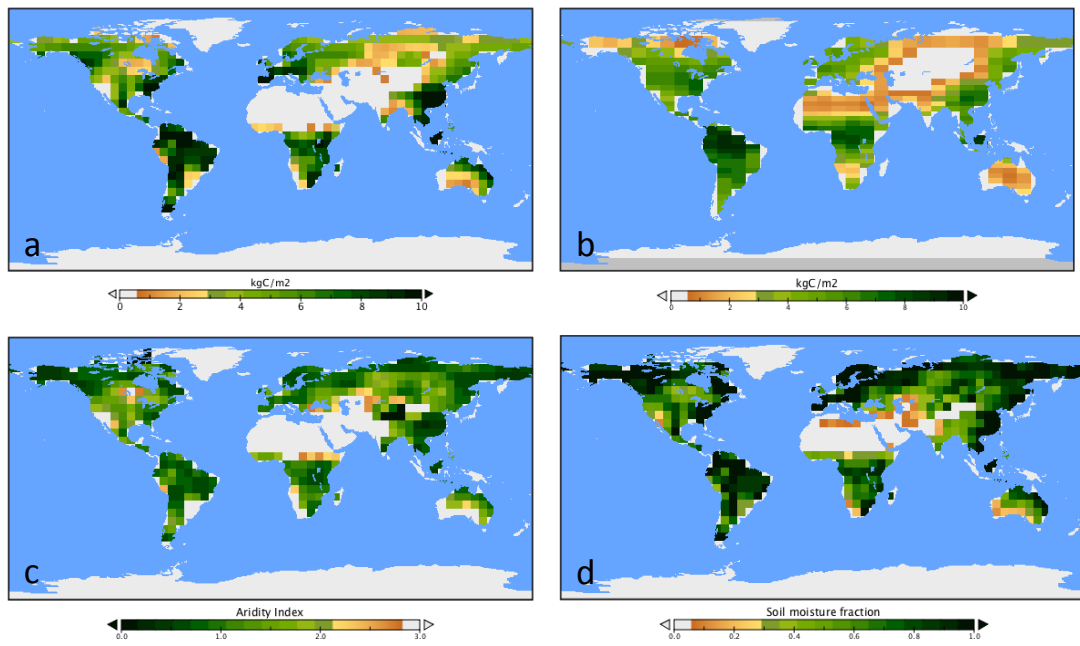
**Figure 3:** Seasonal surface zonal and meridional wind speeds ( $\text{ms}^{-1}$ ). Left: PLASIM-GENIE 50-year average. Centre: long-term average (1981-2010) NCEP/NCAR reanalysis fields (Kalnay et al 1996). Right: difference (PLASIM-NCEP).



995  
 996  
 997  
 998  
 999  
 1000

**Figure 4:** Seasonal incoming surface solar and thermal radiation ( $\text{Wm}^{-2}$ ). Left: PLASIM-GENIE 50-year averages. Centre: long-term average (1981-2010) NCEP/NCAR reanalysis fields (Kalnay et al 1996). Right: difference (PLASIM-NCEP).

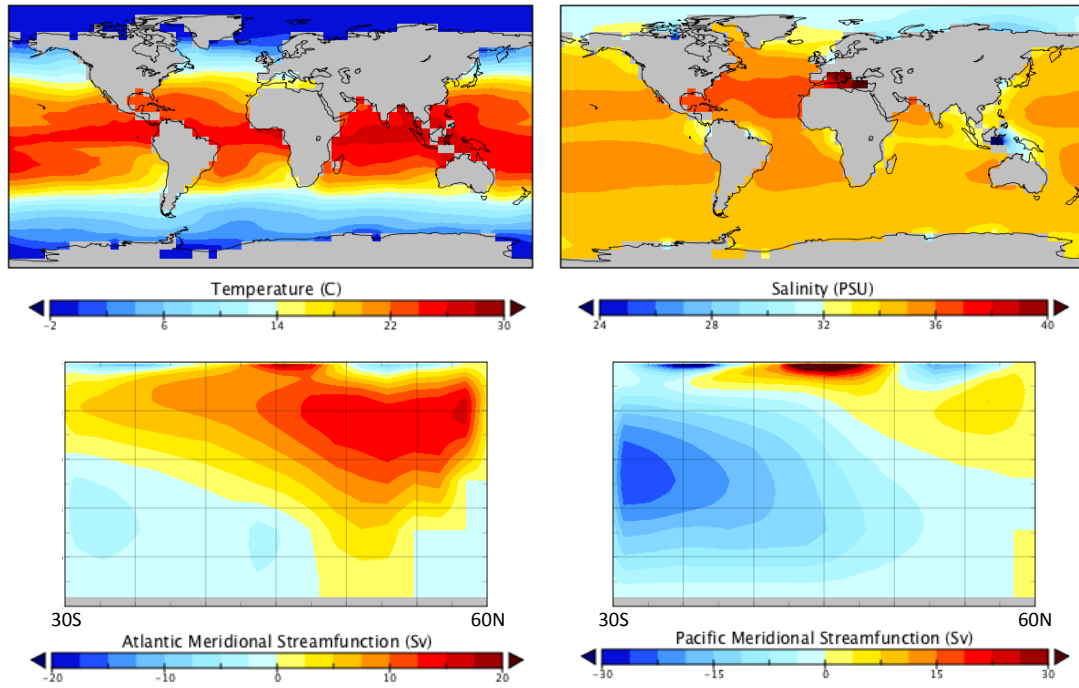
1001



1002  
1003  
1004  
1005  
1006

**Figure 5:** Land surface. a) ENTS vegetation carbon density from PLASIM-GENIE, b) ENTS vegetation carbon density from GENIE-1 (Holden et al 2013a), c) Budyko aridity index N/P and d) soil moisture fraction E/N

1007



1008

1009

1010

1011

1012

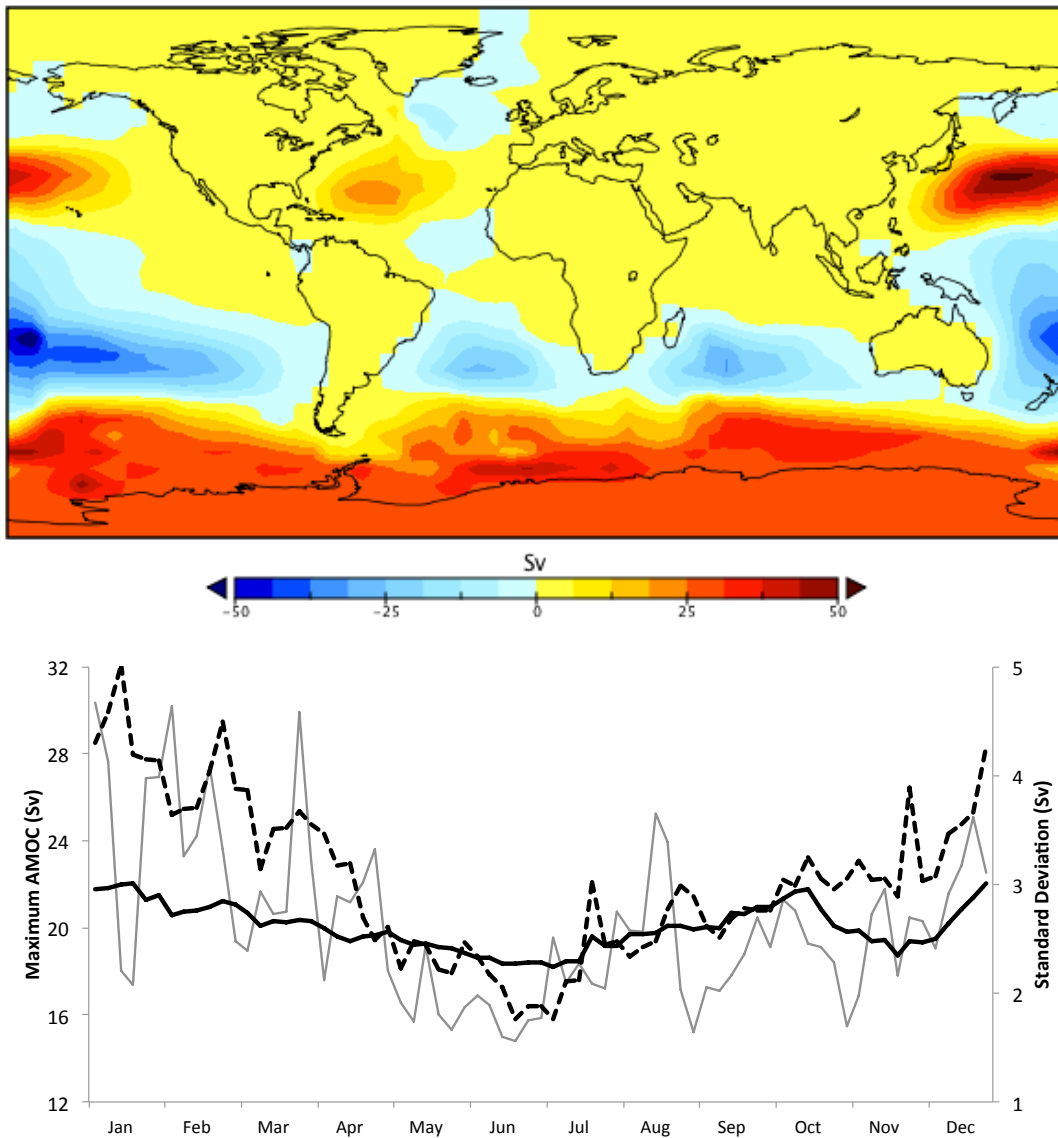
1013

1014

1015

**Figure 6:** Ocean. Upper panels: PLASIM-GENIE simulated surface ocean temperature and salinity. Lower panels: PLASIM-GENIE simulated Atlantic and Pacific meridional stream functions.

1016  
1017



1018  
1019  
1020  
1021  
1022  
1023

**Figure 7:** Upper panel: PLASIM-GENIE barotropic stream function. Lower panel: Wind-driven AMOC variability: solid black 100-year mean, dashed black 100-year standard deviation, solid grey arbitrary year (year 100 of a spin-on simulation)